Materials Research. 2024; 27:e20230446
DOI: https://doi.org/10.1590/1980-5373-MR-2023-0446

Comparative Study Among Graphene Oxide Structures and Their Influence on Electrical Conductivity

***Bruna R. Fenner*[a]*, *Lídia K. Lazzari*[a], *Ademir J. Zattera*[b], *Ruth M. C. Santana*[a]**

[a]*Universidade Federal do Rio Grande do Sul (UFRGS), Av. Bento Gonçalves, 9500, Farroupilha, 91501-970, Porto Alegre, RS, Brasil.*
[b]*Universidade de Caxias do Sul (UCS), R. Francisco Getúlio Vargas, 1130, Petrópolis, 95070-560, Caxias do Sul, RS, Brasil.*

Received: October 12, 2023; Revised: May 08, 2024; Accepted: May 10, 2024

Since graphene and its derivatives discovery, the desire to develop accessible production methods and obtain high-quality materials to enable its production on an industrial scale has increased research interest in this field, and in techniques aiming a deep characterization of these materials. Based on this, the present study proposes a great reduction of time in the process steps of reduced graphene oxide (rGO) production. By using micronized graphite as the precursor, the exfoliation and reduction time were reduced, 67 and 75% respectively, without compromising rGO properties. Regarding the number of layers, the carbon structures presented results between 7 (rGO) and 10 (graphene oxide), being the best result of 8 layers after 10 minutes of exfoliation. Moreover, the electrical conductivity methodology proposed in this article was based on statistical analysis. The electrical conductivity of suspensions with 0.5% w/w of carbon structures was between 3400 and 3700 $\mu S.cm^{-1}$. Thus, this study opens the way for obtaining graphene oxides by the modified Hummers' method and shorter process time in exfoliation and reduction steps using micronized graphite as the precursor, and it also provides a methodology to determine the electrical conductivity of suspensions to assist these materials characterization without prior elimination of the solvent.

Keywords: *Graphene oxide, reduced graphene oxide, Hummers' method, electrical conductivity.*

1. Introduction

Graphene is formed by a monolayer composed of sp^2-bonded carbons packed in a crystalline network. It is considered the thinnest existing material with remarkable properties, such as high thermal conductivity, superior mechanical properties, and excellent electronic properties, contributing to its use in solar panels, sensors, supercapacitors, shape memory composites, biomaterials, among many others in diverse areas of knowledge[1-3]. Also, to the aforementioned advantages, graphene materials present remarkable hydrophobic characteristics, which can be obtained through modified graphene oxide, by its potential for coating on hydrophilic materials application[4,5]. Graphene oxide is produced by controlled oxidation of graphite, and although it has a chemical structure composed of polar chemical groups such as hydroxyls, carbonyls, and epoxy groups, the carbon oxide in the reduced form changes from hydrophilic to hydrophobic system due to the removal of most functional groups during reduction process[6].

The graphene production routes and its derivatives comprise two main processes: bottom-up related to the material synthesis and top-down related to its fragmentation until it reaches the desired scale. The bottom-up process provides many nanomaterials synthesis through the interaction of atoms and/or some molecular species by a set of chemical reactions arising from the technique. The precursor is a liquid or gas that is ionized, dissociated, sublimated, or evaporated and then condensed to form an amorphous or crystalline nanoparticle. This approach produces nanoparticles with fewer defects, homogeneous chemical composition, less contamination, and particles with homogeneous size distribution. In the top-down process, the offset material is a bulk of the same material to be synthesized, which is broken into fragments or particles when an energy source is applied. The applied energy can be either mechanical, chemical, thermal, or even another form of energy, such as laser irradiation. This approach usually results in flakes or smaller particles with varied size distribution and is considered one of the disadvantages of this process[7].

Graphite is the main material used to get graphene and derivatives by top-down processes, composed of stacked carbon layers, which are linked by a weak Van der Walls interaction produced by a displaced π orbital. These carbon layers in graphite are known as graphene layers, and within each layer, there are covalent and metallic bonds. Graphite is anisotropic, being good as an electrical and thermal conductor within the layers (due to in-plane metal bonding) and a poor electrical and thermal conductor perpendicular to the layers (due to van der Walls forces between the layers with distances between them of 3.35 Å). As a result of this anisotropy, the graphene layers can slide into each other, turning graphite into an excellent lubricating and pencil material[8].

*e-mail: bruna.fenner@hotmail.com

The exfoliation method of graphite in deionized water to obtain materials like graphene is explored because these materials present high crystallinity, which is essential for rapid electron transport and is used for electrode applications[9]. Another advantage of this method is that graphene can be produced in the form of inks for subsequent substrate deposition by immersion processes to outturn the desired shape and functionality of materials, such as electrodes, sorbents, and others[10]. Hassoun et al.[11] produced a graphene ink by liquid-phase exfoliation, obtaining small graphene flakes with a high number of active edge points per unit mass, higher than amounts found in graphite or even large graphene flakes. In this study, the separation of graphene layers was performed by ultracentrifugation to produce small sheets, with dimensions below 100 nm, aiming to increase the number of edge points per unit mass, thus believing to optimize the anodes.

Given the difficulty in obtaining graphene, graphene-like materials are researched to increase the yield and enable production on a larger scale. Brodie[12] first demonstrated the synthesis of graphene oxide by adding a part of potassium chlorate to a graphite paste in fuming nitric acid. Staudenmaier[13] improved the process by using concentrated sulfuric acid and fuming nitric acid and added chlorate throughout the reaction. This slight process variation ensured oxidized GO was obtained in a single reaction vessel, which simplified the process. Hummers and Offeman[14] provided the most common method currently used, treatment with potassium permanganate and sodium nitrate in concentrated sulfuric acid oxidizes graphite. Graphite used in chemical reactions, including its oxidation, is in flake form because it is a natural mineral that is purified to remove heteroatomic contamination[15]. This process consists of the chemical oxidation of graphite to graphite oxide, in which several sp^2 carbon atoms are oxidized to sp3 and there is the addition of oxygenated functional groups. Then, the exfoliation of graphite oxide into graphene oxide occurs by separating the stacked two-dimensional sheets containing the oxygenated groups. Lastly, to get reduced graphene oxide, the reduction of oxygenated groups is performed[16,17].

The reduction of graphene oxide is performed by removing oxygen atoms, turning this material closer to graphene, and obtaining the reduced graphene oxide. This step can be done in several means, from thermal reduction to chemical reduction, using different reducing agents, such as borohydrides, aluminum hydrides, amino acids, plant extracts, microorganisms, proteins, hormones, and others[16,18]. Sodium borohydride salt ($NaBH_4$) performs as the reducing agent, which contains a tetrahedral BH^{4-} anion that solubilizes in aqueous and alcoholic media. In the presence of the carbonyl (electrophile) group, the borohydride anion performs a hydride transfer reaction to result in a BH_3 molecule. After stabilization of the BH_3 molecule, the borohydride is established as a hydride transfer agent. This reaction occurs until all the B – H is depleted. Yet, after the reduction step, oxygenated groups remain in the graphene structure, also due to structural defects. The ability of BH^{4-} to reduce the carbonyl group is also limited by the types of carbonyl groups. Simple carbonyl compounds such as aldehyde and ketone are reducible by $NaBH_4$ on alcohol groups, while less reactive carbonyl compounds such as ester or amide are not reducible[18].

Due to its extensive graphite reserves, countries like Brazil, China, and Turkey present an exciting potential for graphene production and graphite derivatives, a material that is being deeply studied due to its unique properties, there is great potential for its use worldwide. Thus, studies related to processes of obtaining less expensive and with a higher yield, allowing its production on an industrial scale, have been growing exponentially, as well as studies contributing with new characterization techniques of these materials or even for the improvement of current ones. To this end, the present study involves a process of obtaining reduced graphene oxide using micronized graphite as a precursor to substitute the usual flake graphite, besides evaluating the time reduction of exfoliation and reduction steps when compared to existing works in literature. During this process, graphene oxide and exfoliated graphene oxide, with three exfoliation times, were obtained, as well as graphite and reduced graphene oxide were characterized according to their physical, chemical, and electrical properties, and compared with commercial graphene oxide. The chemical structures of graphite, graphene oxide, and reduced graphene oxide are present in Figure 1. For the measurement of electrical conductivity of the materials, a methodology was created to determine the electrical conductivity in solution based on statistical analysis.

2. Materials and Methods

Graphene oxides were synthesized from the micronized graphite, with a size ≤ of 20 μm, and were provided by the

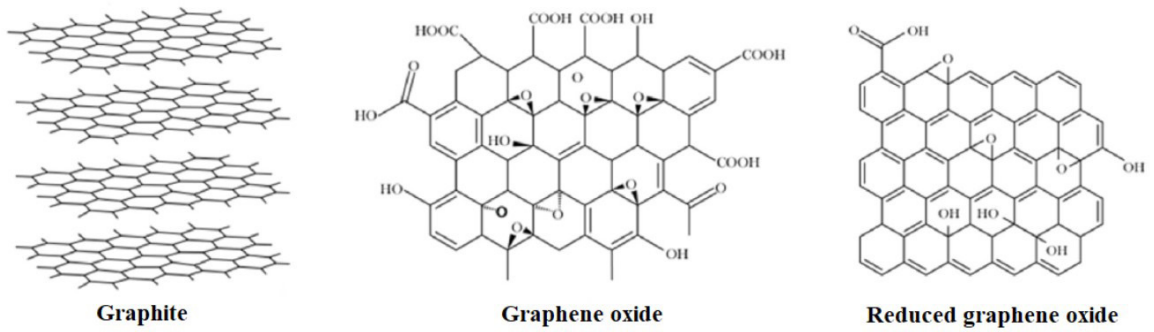

Figure 1. Structure of graphite, graphene oxide, and reduced graphene oxide (rGO).

company Sigma Aldrich, as well as copper (Cu) used as a comparative reference in the characterization of resistivity and electrical conductivity. The reagents needed to get and characterize the produced materials were provided by the company Didática, they were: ethyl alcohol (96%), acetone, sulfuric acid (H_2SO_4, 98%), sodium nitrate ($NaNO_3$), potassium permanganate ($KMnO_4$), hydrogen peroxide (H_2O_2, 5%), barium chloride ($BaCl_2$), sodium borohydride ($NaBH_4$), and grade water. The commercial graphene oxide (cGO), also used as a comparative reference to the carbonaceous structures produced, was provided by the company Timesnano, which presents more than 99% purity, size between 0.5 and 3.0 µm, thickness of the sheets between 0.55 and 1.20 nm and less than three layers. Table 1 presents the nomenclature adopted for the samples produced, as well as their description.

2.1. Obtaining the graphene oxide structures

The initial stage of the carbonaceous structures formation process was to obtain GO through a chemical route using MG as a precursor, followed by the exfoliated graphene oxide (eGO) with different times of exfoliation in deionized water, and finally, the eGO-10 was reduced, obtaining the rGO. The GO was obtained through the modified Hummers' method, adding 110 mL of H_2SO_4 in a beaker with constant stirring. 5 g of graphite, 2.5 g of $NaNO_3$, and 15 g of $KMnO_4$ were added keeping the temperature of the mixture less than or equal to 4°C and constant stirring for 90 minutes. The ratio of graphite (g), H_2SO_4 (mL), and $KMnO_4$ (g) was 1:22:3, similar to the original Hummers' method and its many variations (~1:23:3)[19]. Subsequently, the temperature was adjusted to 35°C for 30 minutes, and then 220 mL of deionized water was joined keeping the temperature below 80°C[6,14].

To discard the free $KMnO_4$ ions, H_2O_2 was added to the obtained solution until the color changed to greenish-yellow. After 15 hours of rest, the solution was washed out with deionized water by centrifugation to remove the H_2SO_4 (4500 rpm; 5 minutes), and the acid detection was made by $BaCl_2$ solution (1% w/w)[20]. The acid-free precipitate was placed in the oven at 50°C for drying. After 10 g of GO was sonicated in 30 g of ethanol for 10, 20, and 30 minutes with a fixed amplitude of 40% measured against the greatest capacity of the equipment (500W) to analyze the number of layers of the samples. For GO chemical reduction, 0.5 g of it was added to 500 mL of deionized water and the mixture was sonicated (10 minutes; 50%). Afterward, a reflux system was set up and the mixture was transferred to a round bottom flask with 5 g of $NaBH_4$. The system was kept at 100°C for 6 hours to complete the reduction process, and the rGO obtained was filtered and dried in ambient air[21].

Table 1. Nomenclature and description of the samples.

Nomenclature	Description of the sample
MG	Micronized graphite.
cGO	Commercial graphene oxide.
GO	Synthesized graphene oxide.
eGO-10	Synthesized graphene oxide + 10 minutes of exfoliation.
eGO-20	Synthesized graphene oxide + 20 minutes of exfoliation.
eGO-30	Synthesized graphene oxide + 30 minutes of exfoliation.
rGO	Synthesized graphene oxide + 10 minutes of exfoliation + reduction.

2.2. Methodology determination for measuring the electrical conductivity of particles in solution with Stabino equipment

For preparation of MG suspensions, 0; 0.05; 0.125; 0.25; 0.5; and 1.0% w/v were added to 10 mL of grade water (conductivity of 0.2 $\mu S.cm^{-1}$ according to supplier). Subsequently, the suspension was sonicated for 30 seconds at 50% amplitude and immediately added to the cylindrical chamber of the equipment to start the conductivity measurements. The equipment used was a Stabino manufactured by Colloid Metrix GmbH (Germany), using a cylindrical chamber of PTFE with an oscillatory piston of 400 µm, and the tests were performed in triplicate. The electrical conductivity measurements are provided by the equipment system in a report.

Analysis of variance (ANOVA) was used to define the method for determining the electrical conductivity of carbonaceous particles in solution. For this, the results of MG in different concentrations and times were statistically analyzed by the Two-Way method due to two existing factors, MG concentration (0; 0.05; 0.125; 0.25; 0.5; 1.0% w/v) and analysis time (0, 50, 100, 150, 200, 250, 300, 350, 400, 450, 500 s). Within that, the electrical conductivity of suspensions containing certain concentrations of MG as a function of the analysis time was evaluated.

2.3. Characterization of carbonaceous structures

The carbonaceous structures were characterized by morphology, structure, composition, and electrical properties. Field emission scanning electron microscopy (SEM/FEG) was performed to analyze the morphology of the carbonaceous samples and energy dispersive spectroscopy (EDS) to identify its composition qualitatively. The analyses were performed in a Tescan, model FEG Mira 3 (Czech Republic), with a voltage of 15 kV. In the EDS analysis, the stub used to deposit the carbonaceous structures is composed mainly of aluminum (Al), besides containing magnesium (Mg) and silicon (Si). Thus, these elements were disregarded in the discussion of the present work. In addition, elements below 1% are classified as trace elements and, because it is a low precision range, these elements were also not considered, except sulfur (S) to analyze the removal of H_2SO_4 from the solid material as explained in section 2.1.

X-ray excited photoelectron spectroscopy (XPS) was performed to identify the composition quantitatively of the carbonaceous structure samples and determine the C/O ratio. An Omicron CHA (concentric hemispherical analyzer model) EA 125 equipment was used with an Al/Kα (1486.6 eV) radiation source and anode operated at 15 kV, 15 mA, 225 W[22-24]. Powder samples were deposited on a copper strip on a molybdenum sample holder. Spectra were obtained at pass energy of 50 eV and 1 eV steps. The core level high resolution of C1s and O1s XPS spectra were obtained with CasaXPS software. The C/O ratio was calculated by area method from the ratio between the areas of the oxygen (A_{O1s})

and carbon (A_{C1s}) signals taking into account their respective Relative Sensitivity Factors (RSF) through Equation 1[25]:

$$C/O = \frac{A_{C1s}}{A_{O1s}} \times \frac{RSF_{O1s}}{RSF_{C1s}} \quad (1)$$

X-ray diffractograms (XRD) were obtained using a Shimadzu equipment - model XRD-6000 (Japan), with monochromatic CuKα radiation of λ = 0.1542 nm, a voltage of 40 kV, and a current of 30 mA. The 2θ scan was performed in an angular range from 2 to 40º, with a 0.05º step and counting time of 2 seconds per step[26]. The powdered samples were analyzed to determine the number of sheets of the carbonaceous structures, which were deposited on a glass slide by solvent evaporation (acetone), the reading area being 10 mm^2. From this test, it was possible to calculate the number of layers of the carbonaceous structures through Bragg's law to calculate the distance between atomic layers and Scherrer's equation to calculate the apparent size of the crystallite, according to Equations 2 and 3[23,27]. The number of graphene layers was calculated by dividing the crystal size by the interlayer distance added to the thickness of one graphene sheet, using Equation 4 proposed by Pavoski et al.[28].

$$d = \frac{n \times \lambda}{2 \times sen\theta} \quad (2)$$

$$L = \frac{K \times \lambda}{\beta \times cos\theta} \quad (3)$$

$$N = \frac{L}{g + d} \quad (4)$$

Where d is the interplanar spacing between the planes (nm), n is an integer, λ is the X-ray wavelength (0.1542 nm), θ is Bragg angle (half the angle between the original beam), L is the apparent size of the crystallite (nm), K is the proportionality constant (0.9), β is the broadening of the diffraction line measured at half height of its maximum intensity (radians), N is the number of layers in the structure and 'g' is the thickness of a graphene sheet (0.1 nm)[28-30].

The particle size was determined by dynamic light scattering (DLS) using a NANO-flex equipment with a 180° DLS system, which measures particle size distributions of suspensions and emulsions in the range from 0.3 nm to 10 µm and concentrations up to 40% by volume. The DLS software was used to extract data from equipment and create the graphs of frequency and particle size distribution. For sample preparation, 0.5% w/v loading was added in 10 mL of grade water and subsequently, the suspension was sonicated for 30 seconds at 50% amplitude. The refractive index values were set at 1.33 and 2.38 for the dispersant (deionized water) and the material (carbon), respectively, according to the study conducted by Amaro-Gahete et al.[31].

Raman spectra of the powdered samples, prepared in the same way as prepared for XRD, were obtained with the aid of a Renishaw inVia Raman spectrometer, using 5% of a 532 nm laser and a 50x magnification lens. The predominant characteristics of graphite and its derivatives were evaluated through the D and G and 2D (also known as G') bands, located in the bands 1320-1350, 1570-1585, and 2640-2680 cm^{-1}, respectively. The D and G bands of graphite and graphene derivatives are related to the defects present in the structure and number of layers of the carbonaceous materials respectively[32,33]. According to Ferrari[34], the G band is used to quantify the number of layers of structures with up to four layers, above that, other methods are used, such as XRD. The 2D band is also used as an indicator of the number of graphene layers but only for a few layers of materials, mostly up to three layers maximum[35].

The Fourier transform infrared spectroscopy (FTIR) analyses were performed in a Nicolet IS10 Termo Scientific (USA) equipment, each spectrum was obtained by 32 scans, with wavenumber from 4000 to 1500 cm^{-1}, by ATR. The electrical conductivity was determined with Stabino equipment and the methodology is described in Section 2.2.

3. Results and Discussion

3.1. Methodology for determining the electrical conductivity by Stabino equipment

The obtained electrical conductivity values of the suspensions with different MG concentrations in grade water are presented in Figure 2 (all data are presented as Table S1 in Supplementary Material), and from these data, an ANOVA table (Table 2) was generated using Statistica software. Due to the high number of particles in the sample solutions with 1.0% MG, it was not possible to measure their electrical conductivity. Possibly there was an agglomeration of particles on the chamber walls, making it impossible to measure and, therefore, the values found for this concentration were not considered for further statistical analysis.

For the variable 'time,' the P-value was higher than 0.05 with no significant difference between the groups, meaning the analysis time does not influence the measured electrical conductivity. For the variable 'concentration of MG' the P-value was lower than 0.05, indicating a significant difference between the groups, that is, the concentration of MG in the suspension influences the measured electrical conductivity. Finally, for the variable 'interaction' (between time and concentration) the P-value was higher than 0.05, indicating no significant difference between the interaction of these factors.

As there was a significant difference in the factor 'MG concentration', it was performed multiple comparisons of means for this from the Tukey HSD test and Unequal N HSD (Table 3), which showed values below the decision limit of 0.00019 (highlighted) for 0.5% of MG, displaying a significant difference. When comparing the concentrations from 0 to 0.5% among all, only 0.5% of MG shows a significant difference in the value found for the electrical conductivity to the other concentrations. When analyzing the other studied concentrations, there is no significant difference between them.

Thus, as a methodology for measuring the electrical conductivity of the carbon structures in solution, dispersions with 0.5% of material were prepared, using grade water as solvent. The dispersion was sonicated for 30 seconds at 50% amplitude and the measurements were made right after.

3.2. Characterization of carbonaceous structures

Micrographs of MG, GO, eGO-30, rGO, and cGO, and their determined compositions by EDS are presented in

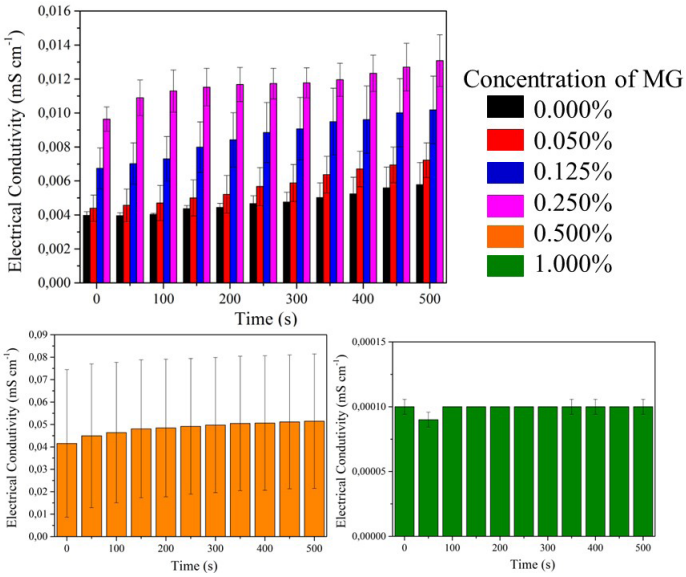

Figure 2. Electrical conductivity of solutions containing different concentrations of MG: a) 0.000-0.250%; b) 0.500%, and c) 1.000% and measuring time.

Table 2. ANOVA table.

Variable	Square sum (SS)	Degree of freedom (gl)	Mean square (MS)	F test	p value
Time (s)	0.043141	10	0.000016	0.0830	0.999916
Concentration of MG (%)	0.000158	4	0.012254	64.4599	0.000000
Interaction	0.000015	40	0.000000	0.0019	1.000000
Error	0.020911	110	0.000190		

Table 3. Tukey test HSD and Unequal N HSD.

		Concentration of MG (%)				
		0	0.050	0.125	0.250	0.500
Concentration of MG (%)	0		0.990299	0.851166	0.225662	0.000115
	0.050	0.990299		0.982670	0.476112	0.000115
	0.125	0.851166	0.982670		0.808186	0.000115
	0.250	0.225662	0.476112	0.808186		0.000115
	0.500	0.000115	0.000115	0.000115	0.000115	

Note: Decision limit 0.00019.

Figure 3. In the MG sample (Figure 3a), it was workable to identify small irregular structures with an average size of approximately 18.7 µm (I), 27.1 µm (II), and 12.5 µm (III), measured with ImageJ software. Moreover, structures composed of several stacked graphene layers can be identified in the image magnification. The GO micrograph (Figure 3b) presents a similarity in some structure's shapes when compared with MG, yet with smaller sizes due to the exfoliation process. The indicated structures present an average size of 5.2 µm (I), 3.6 µm (II), and 2.5 µm (III), and magnifying them, it was possible to identify loose graphene sheets presenting deformations, like the morphology of graphene-based nanosheets via chemical reduction of exfoliated graphite oxide produced by Stankovich et al.[22]. As for the size, Becerra-Paniagua et al.[36] obtained average sizes around 2 µm for graphene oxide also obtained by a variation of the Hummers' method and using flake graphite as precursor.

In Figure 3c, it was possible to perceive the structure of the materials as like the structure of the GO sample (oxide without exfoliation), but with a greater number of clear edges, arising from the exfoliation process. A similar result was presented by Marinho et al.[37] with graphene sheets obtained by graphite oxidation and thermal expansion, referring to entangled graphene structure. In the magnification of eGO-30, it was possible to identify a sheet with transparency, indicating a low thickness and, thus, a small number of stacked graphene sheets. Regarding the samples exfoliated for 10 and 20 min, the results were qualitatively similar to the graphene oxide exfoliated for 30 min.

Within the rGO micrographs (Figure 3f), the reduction with $NaBH_4$ has altered the morphology of the material since the structures changed from larger and particle-shaped structures to more exfoliated structures, also presenting an entangled graphene structure with a crumpled sheet-like appearance, similar to cGO (Figure 3g). In the cGO it was possible to recognize a different structure to the MG, being composed of larger sheets (some over 200 µm wide) and looser, i.e., not stacked as in the MG structure. This might

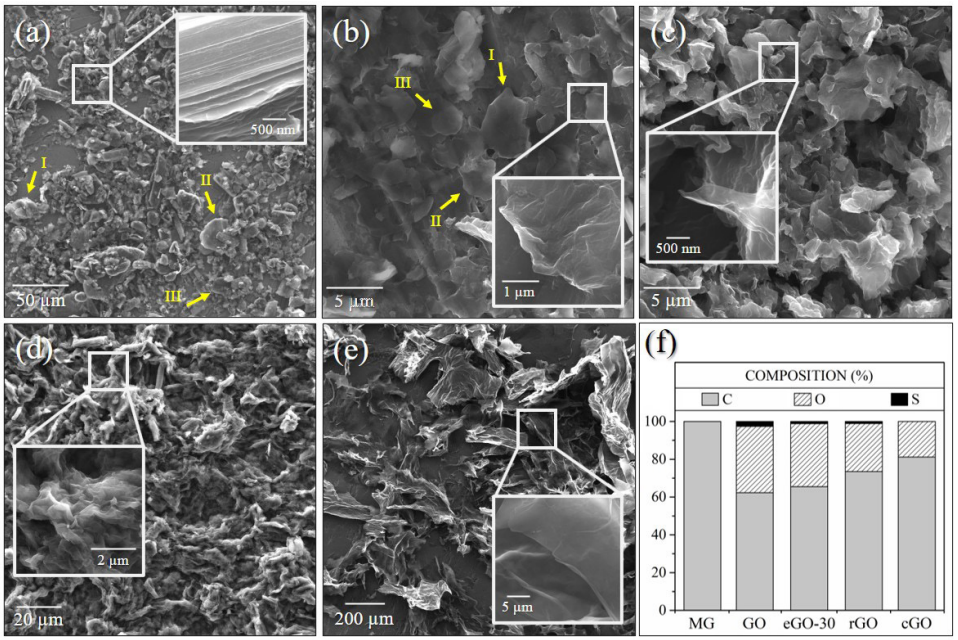

Figure 3. SEM micrographs of MG (a), GO (b), eGO-30 (c), rGO (d), and cGO samples (e); and their compositions by EDS (f).

be due to the precursor selected, which was probably flake graphite – composed of larger particles compared to MG, considering that the supplier of the cGO informed that the method used to obtain this material was Hummers' method (a method that uses flake graphite as a precursor)[15,38,39]. In the magnification, it was also possible to identify loose graphene sheets.

The composition graph regarding the mass percentage of C, O, and S presented in Figure 3f was created from the EDS spectra. About C, the range was from 62.3 to 100%, with the lowest value for GO, this might be due to the higher amount of O, and the highest value was for MG. In the case of O, 35.1% was identified in the GO sample, above even the cGO, which presented 18.8% of O in its composition. This indicates the effective oxidation process, regardless of the number of layers. Considerable amounts of O are seen in eGO-30 and rGO, because of the exfoliation (eGO-30) and reduction (rGO) in the composition of these materials, decreasing the percentage of O to 33.3 and 25.4, respectively. The lower amount of O in sample eGO-30 to GO may be related to the clear surface of sample eGO-30 presenting a higher amount of C to O, which might be explained by the exfoliation process taking place after the oxidation step, being the O inserted in the larger amount on the external surface during oxidation, while the layers were still stacked. As for the rGO, it can be verified the reduction process effectiveness. For cGO, only traces of this element were found, which according to the material's technical sheet provided by the supplier, was also obtained by a variation of the Hummers' method that usually uses H_2SO_4 and $KMnO_4$, justifying the presence of S and K in cGO[14,40,41]. Guerrero-Contreras and Caballero-Briones[38] studied the Hummers' method, reaching an average percentage of 77.7% of C and 20.7% of O, and the materials produced in this study presented 25-35% of O.

Figure 4 presents the wide scan XPS spectrum of the samples MG, GO, rGO, and cGO. All samples showed a peak in the C1s signal, around 284 eV, and a peak at the O1s signal, as described by Marchon et al.[42]. The graphite sample evaluated by Jeon et al.[43] showed the same MG behavior with a sharp peak in C1s and another more subtle peak at O1s signal. For the other samples, the peaks in the same signals are seen, but with distinct intensity. GO presented the peak in the O1s signal more accentuated compared to MG, which led to a balance in the ratio of the C1s and O1s peaks. After the reduction of GO, a decrease in the O1s count in rGO could be verified, which was lower even for cGO.

The C/O ratio is presented in the table of Figure 4. The C/O ratio for MG was 26.62, which suggests there are, approximately 26.62 C atoms for one O. After the oxidation process of MG (material used as a precursor to obtain GO and rGO), GO reached a C/O ratio of 2.89, indicating a significant increase of O fixed in the material. After GO reduction, the amount of O was reduced in the rGO sample, increasing of the C/O ratio (3.55). The GO obtained also presented a C/O ratio lower than cGO, which means that the oxidation process was effective.

Figures 5 and 6 present the core level high resolution of C1s and O1s XPS spectra respectively, as well as its FWHM data in Tables 4 and 5 respectively. The C1s spectra show four components that correspond to carbon atoms in different functional groups. According to Muralikrishna et al.[44], Muthoosamy et al.[45], and Xu et al.[46], the non-oxygenated ring (C–C/C=C) appears at 284.65 eV, the C in C–O bonds at 286.15 eV, the carbonyl C in C=O at 287.63 eV and the carboxyl C in C–C=O at 289.06 eV. A similarity in the shape of the spectrum of GO and cGO can be seen mostly due to the intensity of the C–O peak identified in these samples, which was attenuated with the reduction process, as observed in rGO, and also for MG which is quite weak. Part of the C–O and C=O functional groups of GO were transformed, increasing the proportions of C–C/C=C and O–C=O when their areas were analyzed.

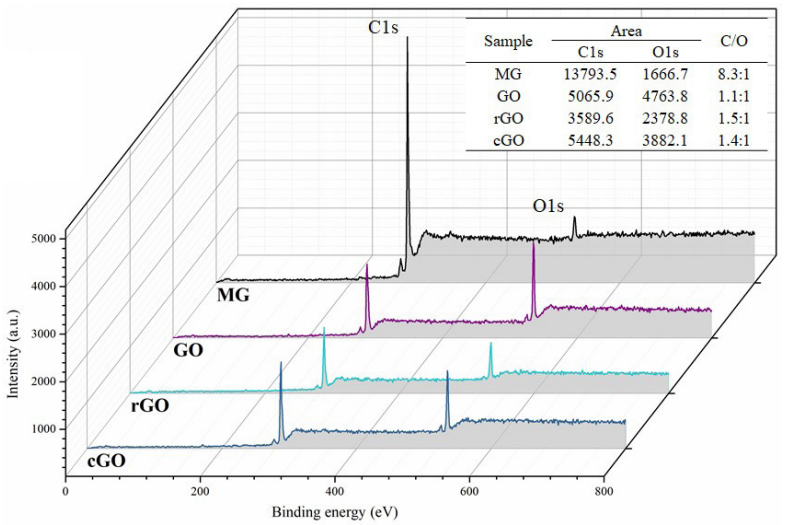

Figure 4. Wide scan XPS spectrum of the samples: MG; GO; rGO; and cGO.

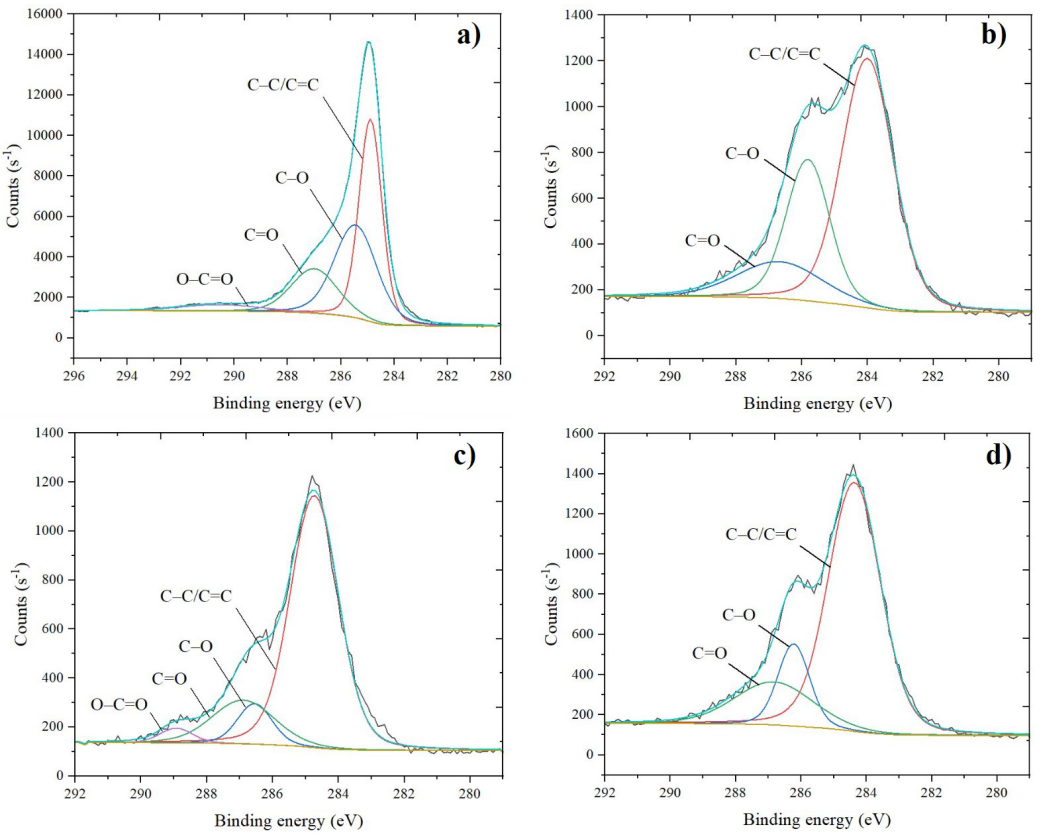

Figure 5. Core level high-resolution C1s XPS spectra of the samples: MG (a); GO (b); rGO (c); and cGO (d).

Table 4. FWHM data of C1s XPS spectra.

Sample	FWHM			
	C–C / C=C	C–O	C=O	O–C=O
MG	1.01	1.88	2.03	3.54
GO	1.73	1.23	2.24	-
rGO	1.86	3.07	1.56	19.65
cGO	1.89	1.14	2.83	-

Table 5. FWHM data of O1s XPS spectra.

Sample	FWHM		
	C–O	C–O–C	C–OH
MG	3.42	-	-
GO	-	3.68	2.36
rGO	-	2.16	2.35
cGO	-	1.28	2.16

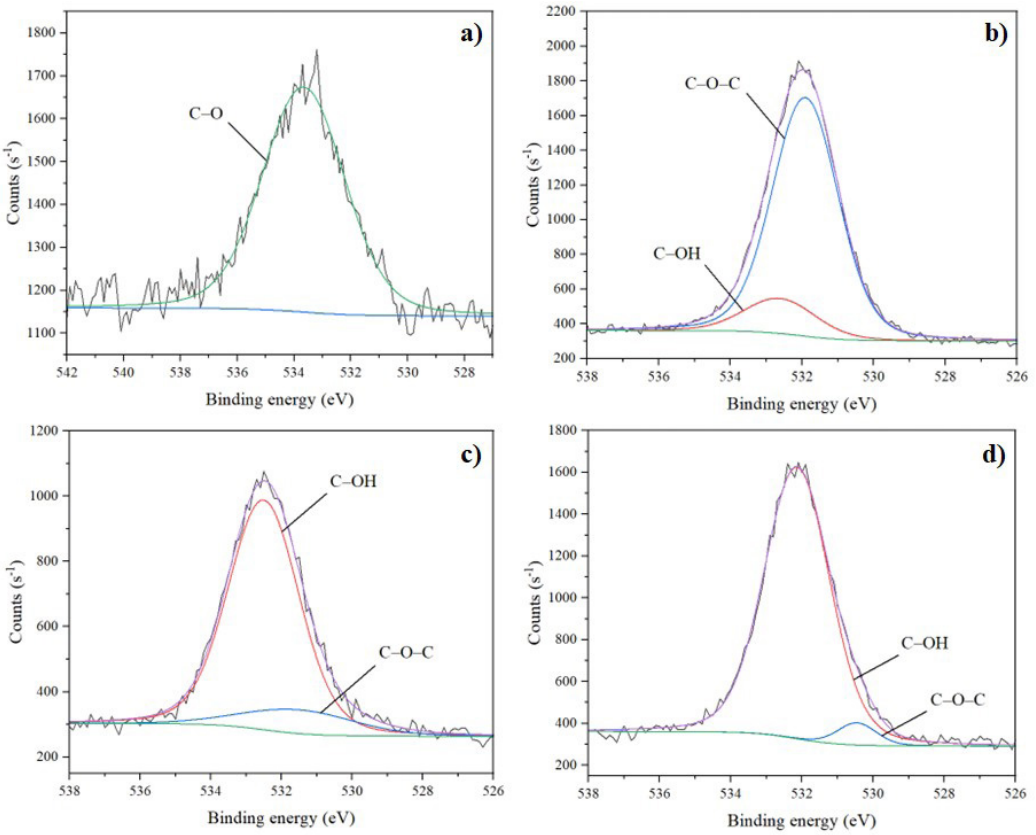

Figure 6. Core level high-resolution O1s XPS spectra of the samples: MG (a); GO (b); rGO (c); and cGO (d).

Jeon et al.[43] attributed the presence of O1s in the graphite spectrum to physically absorbed oxygen. Furthermore, the existence of a single peak at 533.40 eV in MG also could be associated with the presence of the C–O functional group. Regarding oxide samples, the O1s core level high-resolution spectra consist of two O components, C–OH at 532.19 eV and C–O–C at 533.15 eV, as presented by Muralikrishna et al.[44]. The decrease in the peak intensity of C–OH and C–O–C in the rGO (Figure 6c) compared to GO (Figure 6b), confirms that GO was converted into rGO after GO reduction.

The sample behavior presented by this surface analysis corroborates with their compositions determined by EDS (Figure 3), even though MG does not contain O according to the EDS spectra. However, as previously commented, Jeon et al.[43] also identified a peak at O1s for graphite, even if subtle. Regarding the oxides, Fu et al.[47] calculated the C/O ratio using the XPS spectra, obtaining a value of 2.7:1 for graphene oxide, indicating less oxygen retained compared to the GO, rGO, and cGO samples.

Figure 7 presents the FTIR spectra, and the main graphene oxide and its derivatives bands are highlighted, and the peak assignments are presented in Table 6. The spectrum of MG is typical graphite, as obtained by Bindumadhavan et al.[48]. The absorption bands at 3401 and 1386 cm^{-1} correspond to the presence of –OH groups on the surface of rGO and cGO, related to stretching and deformation of the –OH bond, respectively. Also, in these samples and GO, the absorption band identified at 1623 cm^{-1} is associated with the vibrations of unoxidized graphitic double bond (C=C) domains[47-51].

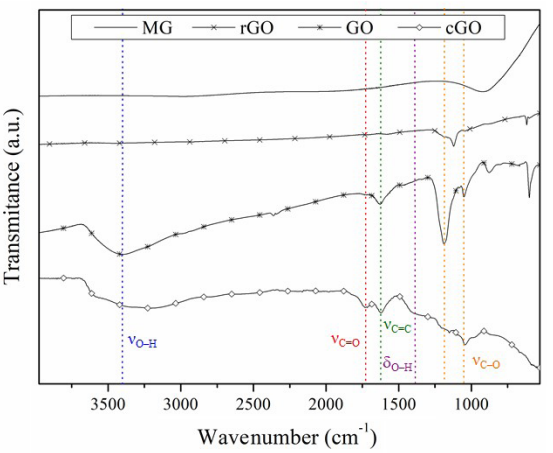

Figure 7. FTIR spectrum of the samples: MG, GO, rGO, and cGO (ν = stretching; δ = deformation).

Table 6. FTIR peak assignments.

Assignment	Wavenumber (cm^{-1})
υ_{O-H}	3401
$\upsilon_{C=O}$	1726
$\upsilon_{C=C}$	1623
δ_{O-H}	1386
υ_{C-O}	1050

Axial vibrations related to C=O bonds are identified at 1726 cm^{-1}, and the bands 1150 and 1050 cm^{-1} are related to C-O axial vibrations, which occur in carboxylic groups (-COOH), according to Lü et al.[52], Liu et al.[6], Kathi and Rhee[53], Ramanathan et al.[54] and Bag et al.[55]. Similar behavior was obtained in the study of graphene synthesis carried out by Marcano et al.[15] and Mai et al.[56]. The intensity of the peaks related to the oxygen functional groups of rGO decreased compared to GO samples, demonstrating the reduction of graphene oxide[57].

The Raman spectra of MG, GO, eGO-10, eGO-20, eGO-30, rGO, and cGO are presented in Figure 8, in which D and G bands were identified, and the 2D band was identified for MG. A highly ordered graphite has only a few active bands visible in the spectra, the vibration phase of the graphite network (G-band) at approximately 1575 cm^{-1}, as well as the (weak) disorder band caused by the graphite edges (D-band) at around 1355 cm^{-1}, as identified for MG. In general, a wider G-band implies greater disorder in the graphite, as well as a wider D-band of higher relative intensity compared to the G-band. 2D-band identified only for MG can be related to the carbon atoms arranged in a hexagonal structure. Possibly, the dissolution of the 2D-band for the graphene oxides, including the commercial one, can be explained by the structural changes caused by the introduction of disorder and structural defects as well as chemical interactions between oxygen and carbon molecules during the oxidation process[58,59].

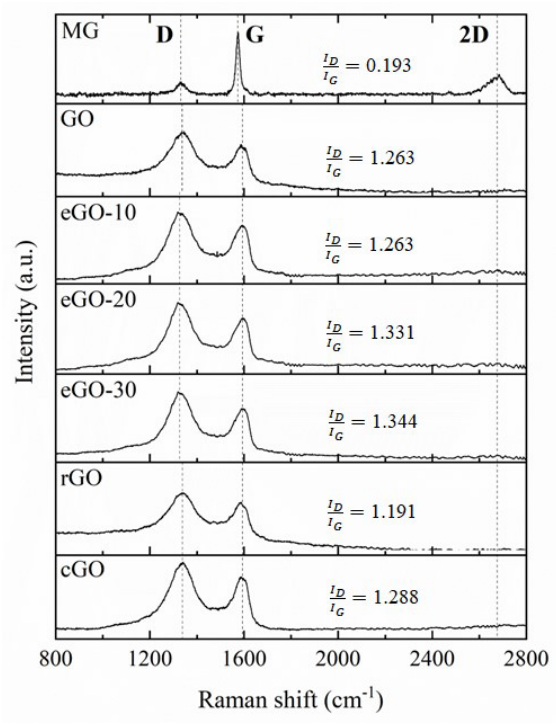

Figure 8. Raman spectra of carbon structures.

For the oxides produced (GO, cGO, eGO-10, eGO-20, eGO-30, and rGO), the D band reached a higher intensity than G, providing the ratio between them greater than an integer. This might be due to defects and topological gaps (vacancies) in these materials by the presence of O in their structures as stated by McAllister et al.[60] and Schniepp et al.[61]. Analyzing the bands individually, a less broad G band with lower intensity is identified in the D band, suggesting that the main defects are evidenced through the D band. When calculating the I_D/I_G of these samples it was verified that GO and eGO-10 displayed the same value of 1.263, which indicates that the defects were not increased with 10 minutes of exfoliation. Nevertheless, the samples eGO-20 and eGO-30 presented a slight intensification of the D band to the G band, indicating that within 20 minutes there was an increase of defects, and within 30 minutes the defects were maintained to eGO-20. Comparing the GO sample with the cGO sample, the same behavior can be observed, as well as a similar ratio between the bands of 1.263 and 1.288. As the value of cGO was higher than GO, it might affirm the synthesized oxide (GO) has fewer defects and vacancies than the commercial oxide (cGO). In rGO, there was an equivalent greater reduction of these defects compared to GO due to the removal of O from its structure after the reduction process.

Figure 9 presents the diffractograms obtained by XRD of the samples MG, cGO, GO, eGO-10, eGO-20, eGO-30, and rGO, and Table 7 shows the data taken from the diffractograms and the calculated data, including the number of layers (N) for each sample. In the diffractogram, a prominent diffraction peak at 2θ = 27.2° can be visualized for MG, which is characteristic of graphite as presented by Perera et al.[62]. For the oxides after the oxidation process, there was a peak shift of the diffraction to the left with 2θ values ranging between 9.9 and 10.7° (Figure 9-I), which

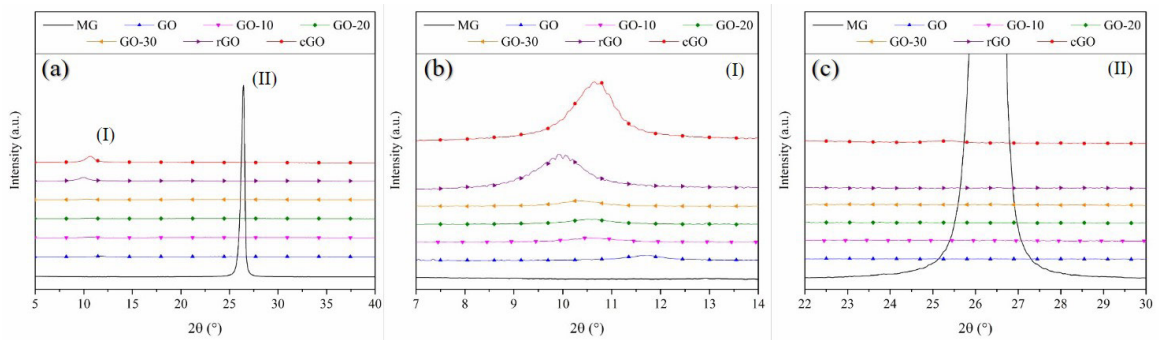

Figure 9. Diffractograms (a) and amplifications of region I (b) and region II (c) of the samples: MG; cGO; GO; eGO-10; eGO-20; eGO-30; rGO.

is characteristic of this material according to Gharib et al.[63] and King et al.[64]. This might be due to the functional groups between the graphitic layers that cause an increase in the interplanar distance[65,66], as presented in Table 7. Analyzing Figure 9-II, all the synthesized samples presented the peak in MG quenched and only the cGO sample had a slight disorder around 25.5°, which was not considered for the calculations.

Correlating the results presented in Table 7 with the diffractograms, it was verified that the MG structure is composed of approximately 97 layers, and after being submitted to the chemical oxidation, it has turned into 11 layers (GO). Analyzing the 'L' values (crystallite size) and 'd' (interplanar distance) of the GO sample to MG, there was a decrease of 'L', about 78% from the initial size, and an increase of 'd' in more than 2.3 times the initial distance. Concerning cGO, a material with 9 graphene layers, GO has 91% of the size of cGO, but a distance above 22% to 'd' of cGO. This relationship is important due to the size of the graphene sheet also influences the properties of the material[67].

Analyzing eGO-10, eGO-20, and eGO-30 samples, it was verified that the exfoliation in ethyl alcohol had no positive influence on the sheet number, considering an increase in layers with an increase in exfoliation time. It indicates the packing of the layers, or still considering that 'L' was greater for eGO-20 and eGO-30 than for eGO-10. Given the small number of samples, the exfoliation in 20 and 30 minutes did not present a considerable difference from 10 minutes. However, evaluating the GO sample and eGO-10 there was a decrease from 11 to 9 layers, since, according to the ISO 80004-13:017 standard[68], the material starts to present properties like graphene when its layer number is below 10. The 10 min exfoliation collaborated with the mechanical separation of the sheets with a high degree of interplanar oxidation that remained stacked, also explaining the results with exfoliation of 20 and 30 minutes.

The rGO presented the lowest number of layers among all, with approximately 8 stacked graphene sheets. Regarding the GO and eGO-10, there was a reduction of 'L' and an increase of 'd' at each step until obtaining rGO, reaching a reduction of 'L' of 82.5% and an increase of 2.7 times in the value of 'd' to MG sample, its precursor, assuming similar results comparing to cGO. This increase in d-spacing is due to the intercalation of water molecules and the generation of oxygen functionality in the interlayer spacing of graphite. The study of Mohan et al.[66] about reduced graphene oxide presents a similar behavior, in which d-spacing increases with increasing reduction time, and the higher the value of 'd' higher the electrical conductivity of the material. According to ISO 80004-13:017[68], analyzing only the number of layers of carbonaceous materials, the cGO, eGO-10, eGO-20, eGO-30, and rGO fit in low-layer graphene for being composed of less than 10 layers.

Perera et al.[62] studied the impact of oxygen on the structure and exfoliation in graphene oxide concerning oxidation time, where it was found values for 'd' between 0.892 and 0.925 nm, for 'L' in the range of 16.9 - 18.3 nm and with this, it was obtained materials with 19 to 20 layers. Comparing these values with the values of the oxides obtained, it can be recognized the interplanar distance was close, but the crystallite size of the study in comparison was around double, which justifies the high number of layers presented by them.

Figure 10 shows the results generated by the DLS software of the GO, rGO, and cGO samples, where the axis 'd' represents the particle size (considered the leaf size), 'Qr' is the distribution curve, and 'q*r' is the frequency that particles of a given size rise. Also, the data generated regarding the representative volumes of these samples according to their respective average sizes are presented. It was not possible to analyze MG by this method due to restrictions of the equipment for measurements at the nanometric scale.

The cGO sample presents a well-concentrated particle size, presenting particles with a size of around 56.2 nm representing 100% of the sample volume. When analyzing

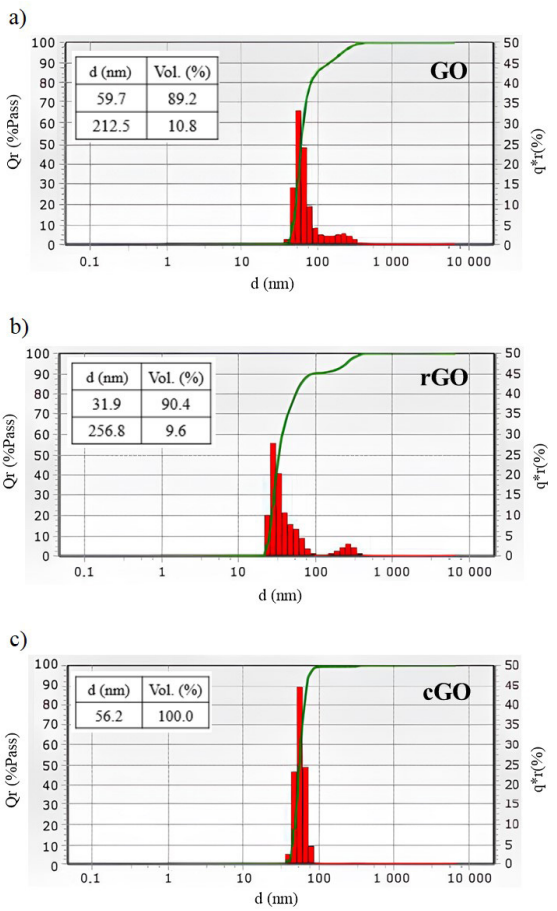

Figure 10. Frequency and particle size distribution of a) GO, b) rGO, and c) cGO by DLS.

Table 7. Data from diffractograms of the samples: MG; cGO; GO; eGO-10; eGO-20; eGO-30; rGO.

Sample	Center 2θ (°)	β	d	L	N
		(rad)	(nm)	(nm)	
MG	27.2	0.199	0.328	41.14	96
GO	11.7	0.891	0.756	897	10
eGO-10	10.55	1.033	0.839	7.73	8
eGO-20	10.5	0.971	0.843	8.22	9
eGO-30	10.3	0.905	0.829	8.82	9
rGO	9.90	1.110	0.894	7.19	7
cGO	1065	0988	0.831	8.08	9

GO and rGO, the first presented a similar value to cGO of 59.7 nm related to 89.2% of the total volume analyzed, and the rest of the particles presented 212.5 nm. On the other hand, rGO presented a particle size smaller than cGO, half the particle size of GO approximately, with an average value of 31.9 nm. The rGO sample presented two particle-size regions with representative volumes, like GO. Frankberg et al.[69] obtained graphene oxide by Hummers' method, but with flake graphite with a particle a size distribution within the largest volume with a size close to 1000 nm, and the smallest volume with size close to 100 nm, as opposed to the present study.

By presenting two particle size representative volumes, as occurred for GO and rGO, it might be concluded there is a need for a particle separation process aiming at the reduction of this particle size variation. With this, it is possible to get a higher-quality material since it presents a lower-size distribution. Even with two representative volumes of particle sizes in the same sample, the values were from 32 to 257 nm. Whereas in the study of Kashyap et al.[65], they evaluated the particle size distribution of graphene oxide at different pHs by DLS, and they obtained an average of 600 nm with a maximum of 1000 nm. Moreover, the particle size behavior of the samples agreed with the behavior of the number of layers found through the diffractograms obtained by XRD.

Figure 11 presents the electrical conductivity of the carbonaceous structures (MG, GO, rGO, and cGO) and Cu in suspension form. The Cu electrical conductivity was used as a reference because it is widely applied in the electrical conductivity field[70]. However, in the literature, the conductivity of Cu is presented in powder form which is around 58.7 x 10^{10} µS.cm^{-1}, while in suspension form with a concentration of 0.5% w/w the conductivity was 678.4 µS.cm^{-1}. This considerable difference might be explained by the Cu conductivity from the literature being measured directly in the solid material, and in this work, a small amount of solid material was in water suspension.

The MG sample presented low conductivity, around 20.1 ± 1.4 µS.cm^{-1}. Regarding GO, there was a considerable increase in conductivity compared to MG (its precursor)

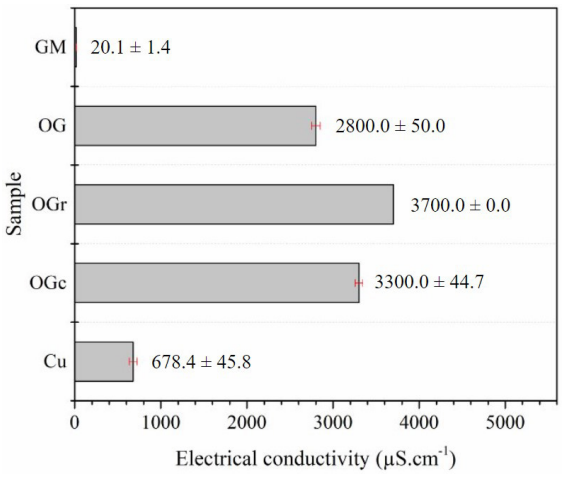

Figure 11. Electrical conductivity of the samples: MG, GO, rGO, cGO, and Cu.

reaching 2800 µS.cm^{-1}, more than 4 times the conductivity of Cu, but lower than cGO (3300 µS.cm^{-1}). This considerable increase can possibly related to the reduction of particle size, mainly regarding the decrease of layer structure. The difference between the electrical conductivity of GO and cGO probably is due its particular characteristics from variables related to methodology and materials used in the synthesis process to obtain both graphene oxides. These variables can affect material characteristics as the size of the sheet, number of layers, defects, a form of the layers, and composition which impact directly electrical conductivity. After the reduction of graphene oxide, it was possible to reach a conductivity of 3700 µS.cm^{-1} for rGO, which was the highest electrical conductivity and presents the best reproducibility among all samples in the test, evaluated by the non-existent deviation. It is important to notice that the electrical conductivity for nanoscale samples (GO, rGO, and cGO) was higher than the microscale samples (MG and Cu) due to the higher surface area of nanoscale materials compared to microscale materials, enhancing the electrical conductivity of the suspension with these nanomaterials. Also, the solubility in water of the samples can affect the result since a homogeneous dispersion in solution supports the electrical conductivity, which may have influenced the electrical conductivity results of Cu and MG compared to GO, rGO, and cGO samples.

Table 8 presents a summary of graphite and oxide sample results to visualize the behavior of electrical conductivity (a) compared to the other results presented in this study. Analyzing the graphs presented, a similar behavior was verified for all properties of the two graphene oxides (GO and cGO) comparing each one of them separately with the rGO. Regarding the process of obtaining rGO from MG based on the results of MG, GO, and rGO, there was an increase in GO electrical conductivity followed by another increase after its reduction. Besides the weak dispersion of MG in water and its surface area being considerably lower when compared to GO and rGO, another factor that may be related to the increase the electrical conductivity is the addition of oxygen in the carbonaceous structure MG, previously mostly composed of C, helping to reduce the surface tension between the oxides and water, as well as their homogeneous dispersion. After the reduction step, a slight decrease of oxygen content in rGO can be observed, but also a considerable increase in electrical conductivity. Combined with that, the behavior of the defects analyzed by I_D/I_G from Raman spectra shows a decrease of electrical conductivity with the increase of defects in oxides structure, which means that there are other factors impacting other factors related to the electrical conductivity of materials.

Correlating the behavior of the electrical conductivity with the interplanar distance (d) from XRD, it was possible to

Table 8. Summary results of the samples: MG, GO, rGO, and cGO.

	Conductivity (µS/cm)	C/O	ID/IG	d (nm)	N
MG	20.1	8.3	0.193	0.328	96
GO	2800	1.1	1.263	0.756	10
rGO	3700	1.5	1.191	0.894	7
cGO	3300	1.4	1.288	0.831	9

observe that the oxide conductivity is higher than MG, which can be related to the addition of oxygen to the carbonaceous structure resulting in a better ion charge transportation through the suspension. The samples respected the following increasing order regarding the 'd' values: MG < GO < cGO < rGO, being the same order followed for the conductivity values. Mohan et al.[66] discussed similar behavior for solid graphene oxides in a solid state regarding d-spacing, which presents a higher electrical conductivity compared to the oxides in suspension. As for the number of layers (N), the electrical conductivity presents the opposite behavior since 'N' is inversely proportional to 'd', meaning that the smaller the number of layers, the greater the electrical conductivity.

4. Conclusions

From the characterization of the carbonaceous structures, it was possible to study the material evolution of the material in each of the specific steps until obtaining the reduced graphene oxide, being characterized by step, exfoliated, and reduced graphene oxide. It was feasible to identify loose sheets for all samples as well as the decrease in size of the MG structures, resulting from an efficient exfoliation of the graphene layers present in the crystalline structure of graphite after the oxidation and exfoliation steps. Within the comparison of the exfoliation times, it was possible to obtain a smaller number of layers with 10 minutes of exfoliation, presenting an efficient reduction of the number of layers and a smaller increase of defects on the surface compared to 20 and 30 minutes. With the reduction step, lower crystallite size and a greater interplanar distance than cGO were achieved, obtaining a lower number of layers for rGO of 7. In addition, the increase of oxygen was seen for rGO compared to GO after the reduction step, as well as compared to commercial graphene oxide through the lower C/O ratio of rGO.

All oxide samples exhibited smaller sizes than the commercial graphene oxide, proving less influence on the electrical properties than the number of layers and composition since the materials' electrical conductivity was superior to the commercial one. Compared to Cu and MG, the samples GO, rGO, and cGO presented approximately 5 times the conductivity of Cu and 175 times the conductivity of MG. Therefore, it was concluded the number of layers has a more prominent influence on the electrical conductivity than the average size of the structures, or even than the C/O ratio since rGO presented a similar ratio to cGO.

Based on the results, it is possible to state the success in obtaining graphene oxides using a high-purity micronized graphite as a precursor, maintaining the usual graphite, H_2SO_4, and $KMnO_4$ (~1:23:3) ratios of the original and modified Hummers' method, even with the reduction time of 2/3 in the exfoliation stage and 3/4 in the reduction stage. Also, it was likely to create a methodology for measuring the electrical conductivity of suspensions with 0.5% concentration valid based on statistical analysis. This method has great potential to facilitate the materials characterization commercialized as suspension without the prior solvent elimination, as there is many types of graphene or oxides currently available on the market.

4.1. Highlights

- Methodology to determine the electrical conductivity of suspensions.
- Use of micronized graphite instead of flake graphite to obtain graphene oxides.
- Increase of electrical conductivity around 165 to 185 times for graphene structures compared to its precursor micronized graphite.
- The best result with an exfoliation time of 10 minutes compared to 20 and 30 minutes.
- Effective reduction of graphene oxide by sodium boron hydride method after only 6 hours.

5. Acknowledgments

This research was supported by the Coordination for the Improvement of Higher Education Personnel (CAPES), the National Council for Scientific and Technological Development (CNPq), and the Foundation for Research Support of the State of Rio Grande do Sul (FAPERGS). The experiment was assisted by Polymers Laboratory, Central Laboratory of Microscopy and Laboratory of Materials Chemical Research at University of Caxias do Sul, and Polymers Laboratory (LAPOL) at Federal University of Rio Grande do Sul.

6. References

1. Aslam S, Sagar RUR, Liu Y, Anwar T, Zhang L, Zhang M, et al. Graphene decorated polymeric flexible materials for lightweight high areal energy lithium-ion batteries. Appl Mater Today. 2019;17:123-9.
2. D'Elia E, Ahmed HS, Feilden E, Saiz E. Electrically-responsive graphene-based shape-memory composites. Appl Mater Today. 2019;15:185-91.
3. Nizami MZI, Takashiba S, Nishina Y. Graphene oxide: a new direction in dentistry. Appl Mater Today. 2020;19:1-14.
4. Gadipelli S, Guo ZX. Graphene-based materials: synthesis and gas sorption, storage and separation. Prog Mater Sci. 2015;69:1-60.
5. Fenner BR, Zimmermann MVG, Silva MP, Zattera A. Comparative analysis among coating methods of flexible polyurethane foams with graphene oxide. J Mol Liq. 2018;271:74-9.
6. Liu Y, Ma JK, Wu T, Wang XG, Huang GR, Liu Y, et al. Cost-effective reduced graphene oxide-coated polyurethane sponge as a highly efficient and reusable oil-absorbent. ACS Appl Mater Interfaces. 2013;5(20):10018-26.
7. Habiba K, Makarov VI, Weiner BR, Morell G. Manufacturing nanostructures. London: One Central Press; 2014. p. 263-92.
8. Chung DDL. Review graphite. J Mater Sci. 2002;37(8):1475-89.
9. Rowley-Neale SJ, Randviir EP, Abo Dena AS, Banks CE. An overview of recent applications of reduced graphene oxide as a basis of electroanalytical sensing platforms. Appl Mater Today. 2018;10:218-26.
10. Segundo JEDV, Vilar EO. Grafeno: uma revisão sobre propriedades, mecanismos de produção e potenciais aplicações em sistemas energéticos. Rev Eletr Mater Proces. 2016;11|(2):54-7.
11. Hassoun J, Bonaccorso F, Agostini M, Angelucci M, Betti MG, Cingolani R, et al. An advanced lithium-ion battery based on a graphene anode and a lithium iron phosphate cathode. Nano Lett. 2014;14(8):4901-6.
12. Brodie BC. On the atomic weight of graphite. Philos Trans R Soc Lond. 1859;14:249-59.
13. Staudenmaier L. Verfahren zur darstellung der graphitsäure. Ber Dtsch Chem Ges. 1898;31(2):1481-7.

14. Hummers WS Jr, Offeman RE. Preparation of graphitic oxide. J Am Chem Soc. 1958;80(6):1339.
15. Marcano DC, Kosynkin DV, Berlin JM, Sinitskii A, Sun Z, Slesarev A, et al. Improved synthesis of graphene oxide. ACS Nano. 2010;4(8):4806-14.
16. Zarbin AJG, Oliveira MM. Nanoestruturas de carbono (nanotubos, grafeno): quo Vadis? Quim Nova. 2013;36(10):1533-9.
17. Park S, Ruoff RS. Chemical methods for the production of graphenes. Nat Nanotechnol. 2009;4(4):217-24.
18. Chua CK, Pumera M. Chemical reduction of graphene oxide: a synthetic chemistry viewpoint. Chem Soc Rev. 2014;43(1):291-312.
19. Yoo MJ, Park HB. Effect of hydrogen peroxide on properties of graphene oxide in Hummers method. Carbon. 2019;141:515-522.
20. Cabrera LC, Baumgarten MGZ, Niencheski LFH, Spengler A. Adaptação do método turbidimétrico para a análise de sulfato. Vetor. 2016;16:7-10.
21. Li B, Liu X, Zhang X, Chai W, Ma Y, Tao J. Strain-induced crystallization of natural rubber/zinc dimethacrylate composites studied using synchrotron X-ray diffraction and molecular simulation. J Polym Res. 2015;22(2):1-6.
22. Stankovich S, Dikin DA, Piner RD, Kohlhaas KA, Kleinhammes A, Jia Y, et al. Synthesis of graphene-based nanosheets via chemical reduction of exfoliated graphite oxide. Carbon. 2007;45(7):1558-65.
23. Lavoratti A, Zattera AJ, Amico SC. Mechanical and dynamic-mechanical properties of silanized graphene oxide/epoxy composites. J Polym Res. 2019;26(6):1-10.
24. Das NM, Singh AK, Ghosh D, Bandyopadhyay D. Graphene oxide nanohybrids for electron transfer-mediated antimicrobial activity. Nanoscale Adv. 2019;1(9):3727-40.
25. Kovtn A, Jones D, Dell'Elce S, Treossi E, Liscio A, Palermo V. Accurate chemical analysis of oxygenated graphene-based materials using X-ray photoelectron spectroscopy. Carbon. 2019;143:268-75.
26. Lavoratti A, Zattera AJ, Amico SC. Mechanical and dynamic-mechanical properties of silane-treated graphite nanoplatelet/epoxy composites. J Appl Polym Sci. 2018;135(45):46724.
27. Borsoi C, Ornaghi HL Jr, Scienza LC, Zattera AJ, Ferreira CA. Isolation and characterisation of cellulose nanowhiskers from microcrystalline cellulose using mechanical processing. Polym Polymer Compos. 2017;25(8):563-70.
28. Pavoski G, Maraschin T, Fim FC, Balzaretti NM, Galland GB, Moura CS, et al. Few layer reduced graphene oxide: evaluation of the best experimental conditions for easy production. Mater Res. 2017;20(1):53-61.
29. Cullity BD, Stock SR. Elements of X-ray diffraction. 3rd ed. Upper Saddle River: Prentice Hall; 2001.
30. Osváth Z, Darabont A, Nemes-Incze P, Horváth E, Horváth ZE, Biró LP. Graphene layers from thermal oxidation of exfoliated graphite plates. Carbon. 2007;45(15):3022-6.
31. Amaro-Gahete J, Benítez A, Otero R, Esquivel D, Jiménez-Sanchidrián C, Morales J, et al. A comparative study of particle size distribution of graphene nanosheets synthesized by an ultrasound-assisted method. Nanomaterials. 2019;9(2):152.
32. Ferrari AC, Meyer JC, Scardaci V, Casiraghi C, Lazzeri M, Mauri F, et al. Raman spectrum of graphene and graphene layers. Phys Rev Lett. 2006;97(18):187401.
33. Hong J, Park MK, Lee EJ, Lee DE, Hwang DS, Ryu S. Origin of new broad Raman D and G Peaks in annealed graphene. Sci Rep. 2013;3(1):2700.
34. Ferrari AC. Raman spectroscopy of graphene and graphite: disorder, electron-phonon coupling, doping and nonadiabatic effects. Solid State Commun. 2007;143(1-2):47-57.
35. Malard LM, Pimenta MA, Dresselhaus G, Dresselhaus MS. Raman spectroscopy in graphene. Phys Rep. 2009;47(3):51-87.
36. Becerra-Paniagua DK, Sotelo-Lerna M, Hu H. Highly oxidized and exfoliated graphene using a modified Tour approach. J Mater Sci Mater Electron. 2019;30:3973-83.
37. Marinho B, Ghislandi M, Tkalya E, Koning CE, With G. Electrical conductivity of compacts of graphene, multi-wall carbon nanotubes, carbon black, and graphite powder. Powder Technol. 2012;221:351-8.
38. Guerrero-Contreras J, Caballero-Briones F. Graphene oxide powders with different oxidation degree, prepared by synthesis variations of the Hummers method. Mater Chem Phys. 2015;153:209-20.
39. Kang JH, Kim T, Choi J, Park J, Kim YS, Chang MS, et al. Hidden second oxidation step of hummers method. Chem Mater. 2016;28(3):756-64.
40. Gao W, Alemany LB, Ci L, Ajayan PM. New insights into the structure and reduction of graphite oxide. Nat Chem. 2009;1(5):403-8.
41. Yu H, Zhang B, Bulin C, Li R, Xing R. Ultrastructural characterization of the lower motor system in a mouse model of Krabbe disease. Sci Rep. 2016;6:1-7.
42. Marchon B, Carrazza J, Heinemann H, Somorjai A. TPD and XPS studies of O_2, CO_2, and H_2O adsorption on clean polycrystalline graphite. Carbon. 1988;26(4):507-14.
43. Jeon I, Choi H, Ju MJ, Choi IT, Lim K, Ko J, et al. Direct nitrogen fixation at the edges of graphene nanoplatelets as efficient electrocatalysts for energy conversion. Sci Rep. 2013;3(1):2260.
44. Muralikrishna S, Sureshkumar K, Varley TS, Nagaraju DH, Ramakrishnappa T. In situ reduction and functionalization of graphene oxide with l -cysteine for simultaneous electrochemical determination of cadmium(ii), lead(ii), copper(ii), and mercury(ii) ions. Anal Methods. 2014;6(21):8698-705.
45. Muthoosamy K, Bai RG, Abubakar IB, Sudheer SM, Lim HN, Loh H, et al. Exceedingly biocompatible and thin-layered reduced graphene oxide nanosheets using an eco-friendly mushroom extract strategy. Int J Nanomedicine. 2015;10:1505-19.
46. Xu C, Shi X, Ji A, Shi L, Zhou C, Cui Y. Fabrication and characteristics of reduced graphene oxide produced with different green reductants. PLoS One. 2015;10(12):e0144842.
47. Fu C, Zhao G, Zhang H, Li S. Evaluation and characterization of reduced graphene oxide nanosheets as anode materials for lithium-ion batteries. Int J Electrochem Sci. 2013;8(5):6269-80.
48. Bindumadhavan K, Srivastana S, Srivastana I. Green synthesis of graphene. J Nanosci Nanotechnol. 2013;13(6):4320-4.
49. Silverstein RM, Webster FX, Kiemle DJ, Bryce DL. Spectrometric identification of organic compounds. 8th ed. Hoboken: Wiley; 2015.
50. Du W, Jiang X, Zhu L. From graphite to graphene: direct liquid-phase exfoliation of graphite to produce single- and few-layered pristine graphene. J Mater Chem A Mater Energy Sustain. 2013;1(36):10592-606.
51. Zhu Q, Pan Q, Liu F. Facile removal and collection of oils from water surfaces through superhydrophobic and superoleophilic sponges. J Phys Chem. 2011;115:17464-70.
52. Lü X, Cui Z, Wei W, Xie J, Jiang L, Huang J, et al. Constructing polyurethane sponge modified with silica/graphene oxide nanohybrids as a ternary sorbent. Chem Eng J. 2016;284:478-86.
53. Kathi J, Rhee KY. Surface modification of multi-walled carbon nanotubes using 3-aminopropyltriethoxysilane. J Mater Sci. 2008;43(1):33-7.
54. Ramanathan T, Fisher FT, Ruoff RS, Brinson LC. Amino-functionalized carbon nanotubes for binding to polymers and biological systems. Chem Mater. 2005;17(6):1290-5.
55. Bag DS, Dubey R, Zhang N, Xie J, Varadan VK, Lal D, et al. Chemical functionalization of carbon nanotubes with 3-methacryloxypropyltrimethoxysilane (3-MPTS). Smart Mater Struct. 2004;13(5):1263-7.
56. Mai T, Thuc NCH, Thuc HH. Preparation of graphene nano-layer by chemical graphitization of graphite oxide from exfoliation and preliminary reduction. Fuller Nanotub Carbon Nanostruct. 2015;23(8):742-9.

57. Shang YU, Zhang D, Liu Y, Guo C. Preliminary comparison of different reduction methods of graphene oxide. Bull Mater Sci. 2015;38(1):7-12.
58. Kudin KN, Ozbas B, Schniepp HC, Prud'homme RK, Aksay IA, Car R. Raman spectra of graphite oxide and functionalized graphene sheets. Nano Lett. 2008;8(1):36-41.
59. Tuinstra F, Koenig JL. Raman spectrum of graphite. J Chem Phys. 1970;53(3):1126-30.
60. McAllister MJ, Li J, Adamson DH, Schniepp HC, Abdala AA, Liu J, et al. Single sheet functionalized graphene by oxidation and thermal expansion of graphite. Chem Mater. 2007;19:4396-404.
61. Schniepp HC, Li J, McAllister MJ, Sai H, Herrera-Alonso M, Adamson DH, et al. Functionalized single graphene sheets derived from splitting graphite oxide. J Chem Phys B. 2006;110:8535-9.
62. Perera D, Abeywickrama A, Zen F, Colavita PE, Jayasundara DR. Evolution of oxygen functionalities in graphene oxide and its impact on structure and exfoliation: an oxidation time based study. Mater Chem Phys. 2018;220:417-25.
63. Gharib A, Fard LV, Pesyan NN, Roshani M. A new application of nano-graphene oxide (NGO) as a heterogeneous catalyst in oxidation of alcohols types. Chem J. 2015;1(4):151-8.
64. King AAK, Davies BR, Noorbehesht N, Newman P, Church TL, Harris AT, et al. Ultrastructural characterization of the lower motor system in a mouse model of Krabbe disease. Sci Rep. 2016;6(1):1-6.
65. Kashyap S, Mishra S, Behera SK. Aqueous colloidal stability of graphene oxide and chemically converted graphene. J. Nanopart. 2014;2014:1-6.
66. Mohan VB, Brown R, Jayaraman K, Bhattacharyya D. Characterisation of reduced graphene oxide: effects of reduction variables on electrical conductivity. Mater Sci Eng B. 2015;193:49-60.
67. Li Y, Chiang W. Intercalation-assisted longitudinal unzipping of carbon nanotubes for green and scalable synthesis of grapheme nanoribbon. Sci Rep. 2016;6:1-12.
68. ISO: International Organization for Standardization. ISO/TS 80004-13:2017. Geneva: ISO; 2017.
69. Frankberg EJ, George L, Efimov A, Honkanen M, Pessi J, Levanen E. Measuring synthesis yield in graphene oxide synthesis by modified hummers method. Fuller Nanotub Carbon Nanostruct. 2015;23(9):755-9.
70. Berman R, MacDonald DKC. The thermal and electrical conductivity of copper at low temperatures. Proc R Soc Lond. 1951;211:122-8.

Supplementary Material

The following online material is available for this article:

Table S1. Electrical conductivity of solutions containing different concentrations of MG and measuring time.